16th World Conference on Earthquake Engineering, 16WCEE 2017
Santiago Chile, January 9th to 13th 2017
Paper N° 1716 (Abstract ID)
Registration Code: S- S1462563954

Correction of acceleration records obtained from free vibration tests on base isolated buildings

A. Athanasiou[(1)], G. Oliveto[(2)]

[(1)] *Postdoctoral researcher, University of Catania, athanasiou@dica.unict.it*
[(2)] *Professor, University of Catania, goliveto@dica.unict.it*

Abstract

A three-story reinforced concrete building in Augusta (Sicily, Italy), isolated at the base and designed according to the provisions of the latest Italian seismic regulations, was subjected to a series of push and sudden release tests in March 2013. The isolation system consisted of 16 high damping rubber bearings and 20 low friction sliding bearings. The release tests were performed at low amplitudes to ensure that no damage would occur in the building; the imposed displacements varied from 5.8cm to 11.7cm (isolator demand γ_{max}=0.39-0.78). During the tests, the displacements at the isolation level were measured along with the accelerations at each floor of the building. Once the tests were completed, the observed structural response was used for the assessment of the properties of the isolation system. Before input in analyses, the signals were treated for the removal of low frequency noise using a simple baseline fitting scheme. The developed signal processing scheme consists in defining the duration of the main event, removing the background noise and using polynomial curves for the adjustment of the signal reference baseline. The method does not require significant computational effort and accounts for boundary conditions, provided that these are known. The polynomial coefficients used in the baseline fitting of the signals are determined from the boundary conditions; namely the initial and end accelerations, velocities and displacements. The deterministic definition of the polynomial coefficients and the recovery of permanent displacements enforces the reliability of the method and makes it an attractive alternative to high pass filtering, which instead requires proficient users and includes a lot of subjectivity in the filter parameter selection. The proposed baseline scheme is applied herein for the adjustment of the absolute and relative acceleration signals obtained from test 9, one of the tests with the highest initial input (u_0=10.1cm). Implementation of the method provides the adjusted response in terms of absolute and relative floor accelerations, velocities and displacements. The processed absolute accelerations and velocities are zero when the motion starts and when the motion ceases; while the absolute ground floor displacement equals the experimental (measured) initial displacement at the beginning of motion and the experimental residual displacement at the end of motion. The predicted ground floor displacement matches very satisfactorily the displacement measurement. The developed method is implemented moreover on the relative to the base acceleration signals, for the evaluation of the relative displacement and velocity response of the superstructure. The method assures that the relative response is zero at the beginning and end of motion, since the superstructure remains elastic under such small excitation. The relative response is evaluated in two ways: (i) subtracting the adjusted ground floor response from the adjusted upper floor response and (ii) processing the raw relative motions. The implementation of methodologies (i) and (ii) provides identical relative accelerations and velocities, enforcing the reliability of the method. The relative displacements are high pass filtered to remove the effect of long period noise in the second half period of motion, where the signal amplitude is significantly small and the noise is probably predominant.

Keywords: base isolation, field tests, baseline fitting, correction polynomials, low frequency noise

1. Introduction

Signal processing aims to the removal of noise from the strong motion data and the extraction of valuable information, such as peak ground characteristics and response spectra. However, considering the arbitrary nature of the noise, it becomes clear that no method can recover the original, uncontaminated signal. Noise causes distortion of the signal in a wide frequency range. The influence of noise is more dramatic in the low (<1Hz) and high (>20Hz) frequency range, where the signal to noise ratio tends to be significantly lower. The signal to noise ratio (SNR) is defined as the ratio of the signal power to the noise power and it is a measure of the signal contamination. The lower the SNR, the more contaminated the data. The effect of long period noise, which is basically the distortion of the reference baseline, cannot be detected easily in the acceleration record. However, once the acceleration is integrated to provide velocities and displacements its influence becomes clear; uncorrected accelerations generate un-physical velocities and displacements. Given the increased engineering interest towards performance based design strategies and towards structures that respond in the long period range (high-rise buildings, bridges, isolated structures) the correction of records for low frequency noise becomes of major importance for the production of plausible displacements and realistic response spectra at the long period range. Low frequency noise originates in instrument errors, constant acceleration drifts, background noise and manipulation errors [1]. An overview of signal processing methodologies for the treatment of long period noise can be found in [2]. Low frequency noise can be treated using low cut (or high pass) filters, and/or baseline fitting schemes. When low cut filters are applied to the signal, the signal components with frequencies below the selected cut-off frequency are removed. The generated response is very sensitive to the selection of the cut-off frequency. On the other hand, baseline fitting schemes can be considered as *'low-cut filters of unknown frequency characteristics'* [2]. They consist in the adjustment of the distorted acceleration, velocity and displacement reference lines using straight or curved lines. In [1] Chiu presents a combination of baseline and filtering procedures for the effective removal of the long period noise. His algorithm provides reliable results and requires less computational effort than the established processing routine developed in the '70s by Trifunac and Lee [3]. Herein, a baseline fitting method is implemented for the removal of the low frequency noise from the free vibration Augusta records.

2. Case study - the Augusta base isolated building

The Augusta building consists of a basement, two stories above the ground level and a penthouse. The structure is 35.70m long and 16.00m wide, the maximum height above the ground level is 10.50m and the basement story height is 3.60m. Pictures of the building exterior are shown in Fig. 1.

(a) (b)
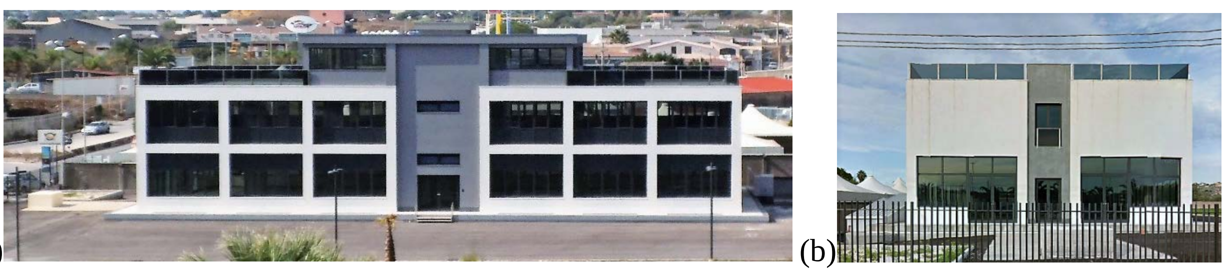

Figs 1 (a) and (b) – East and south views of the Augusta building.

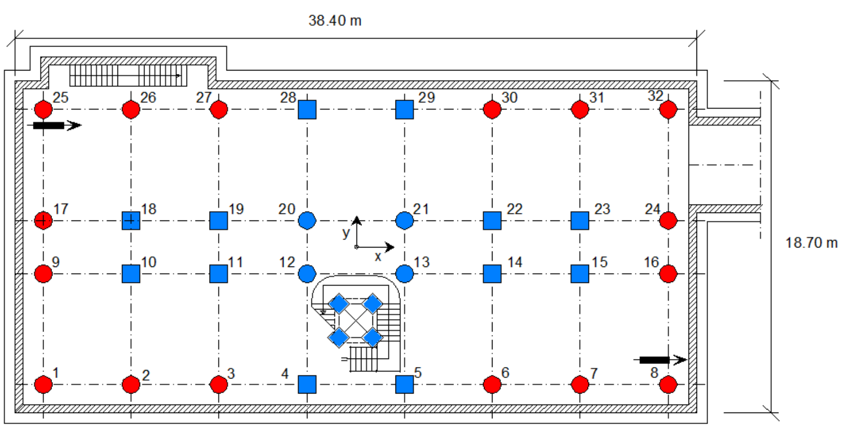

Fig. 2 – Plan view of the Augusta base isolation system. The HDRB are shown in red while the LFSB are shown in blue. The position of the transducer rods, measuring the displacement at the top and bottom of the corner HDRB 25 and 8 is indicated by arrows.

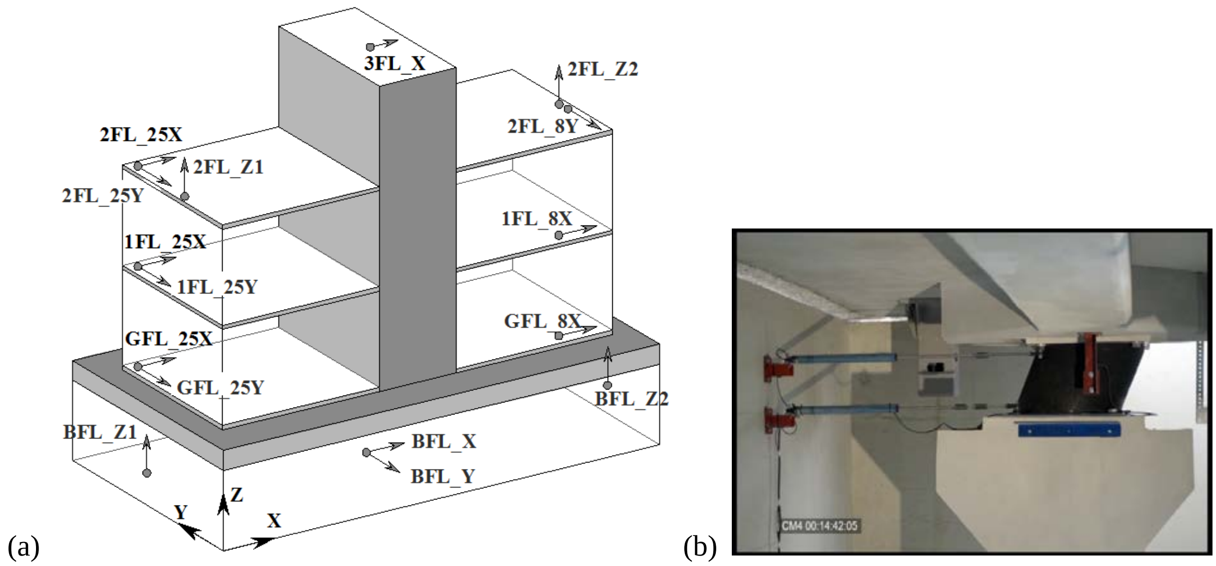

Fig. 3 – (a) Schematic accelerometers layout and (b) displacement sensors used in the measurement of the isolators deformations during the Augusta tests.

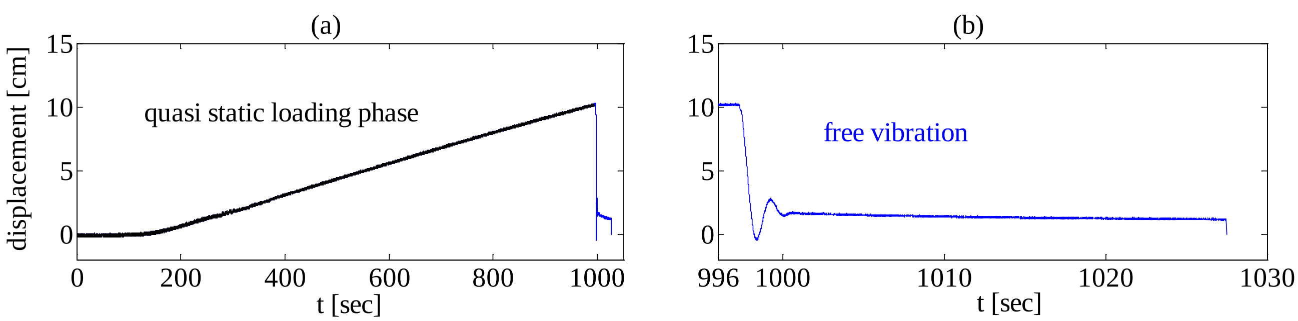

Fig. 4 – Longitudinal displacement measured at the corner isolator 25 of the Augusta building; full and free vibration record for test 9 (u_0 = 10.1cm, γ_{max} = 0.67), sub-plots (a) and (b).

The foundation lies predominantly on deposits of stiff clay, i.e. a site of class B [4]. The building is isolated at the base; the isolators provide the structure with lateral flexibility so that the latter can withstand the horizontal forces induced during strong ground motion. The isolation plane runs along the top of the pillars of the basement story slightly above the ground level and is composed by 16 High Damping Rubber Bearings (HDRB) and 20 Low Friction Sliding Bearings (LFSB) produced by FIP Industriale (products SI-N 500/150, VM 25-150-200/600/600), Fig. 2.

A set of ten release tests were performed on the Augusta building on March 2013 [5]. During the tests the building was displaced statically from its initial position and then it was left to oscillate. The release tests were performed at low amplitudes to ensure that no damage would occur in the building; the imposed displacements varied from 5.8cm to 11.7cm (γ_{max}=0.39-0.78). The testing apparatus consisted of the loading device, the measurement equipment and the data acquisition system. The loading device consisted of a reaction wall, a hydraulic jack, a sudden release device and a load cell and could apply a maximum force of approximately 2000 kN [6]. The force was applied along the long direction of the building (direction x, Fig. 2). The histories of the loading force, displacements and accelerations were recorded throughout the experiments. The horizontal and vertical accelerations were measured at the various floor levels using 16 channels, shown in a schematic layout in Fig. 3(a). The accelerometers used for the recording of the absolute acceleration response were the SA-107LN model produced by COLUMBIA Research Labs Inc. The horizontal displacements were measured below and above two corner isolators using the Penny and Giles linear displacement sensor SLS320/400, see Fig. 2 and Fig. 3(b).

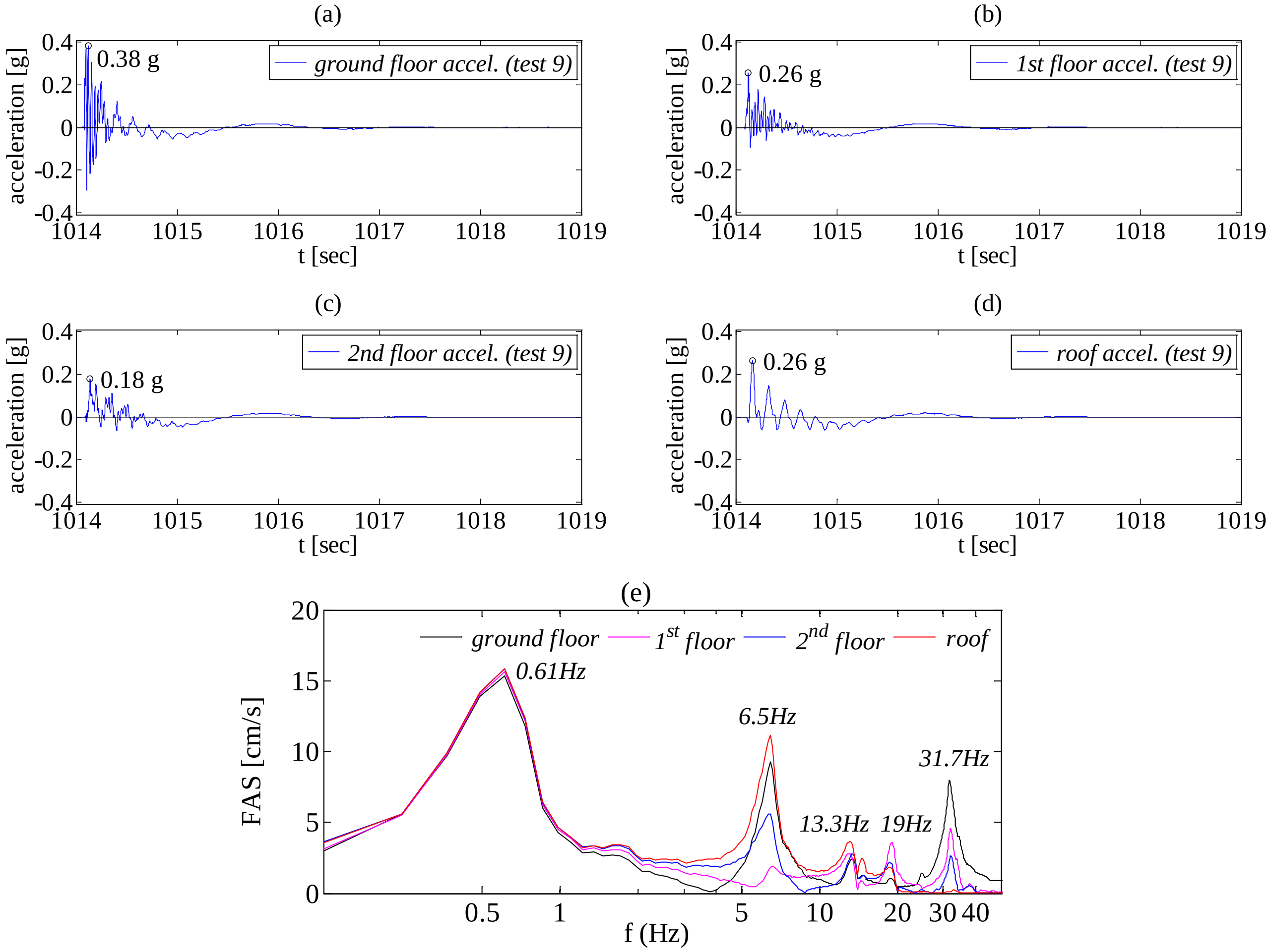

Fig. 5 – (a) to (d). Longitudinal acceleration signals recorded at the Augusta building during test 9 at stations GFL-25X, 1FL-25X, 2FL-25X, 3FL-X shown in Fig. 3(a).
(e) Fourier Amplitude Spectra of the accelerations shown in sub-plots (a) to (d).

2.1 Displacement records

Figs 4 (a) and (b) show the longitudinal displacement measured at the rubber isolator 25 during test 9, Figs 2 and 3(b). Test 9 was among the tests with the higher initial displacement (u_0 = 10.1cm, γ_{max} = 0.67). Fig. 4 (a) shows how the building was pushed quasi-statically for 1000sec (approx. 17min) to a displacement of 10.1cm. As soon as the building was released it started oscillating. However, the free vibration response was damped rapidly and the system came to a rest with a residual displacement. A creep behavior was observed after cessation of motion; this could be attributed to the elastomer. After completion of each test the building was re-centered to the initial, zero displacement, equilibrium position by means of a simple re-centering mechanism. The displacement diagrams provide valuable information about the isolation system, such as estimates of the damped period of vibration T_{1D} and the equivalent damping ratio ζ_{eq}. The damping ratio ζ_{eq} accounts for energy dissipation in both rubber and friction bearings. For test 9 T_{1D}=1.95s (time elapsed between the first two positive peaks) or T_{1D}=1.65s (time elapsed between the first two negative peaks) and equivalent damping ratio ζ_{eq} =20.8% (evaluated from the first two displacement peaks using the logarithmic decrement rule [7]).

2.2 Acceleration records

Figs 5(a) to (d) show the longitudinal acceleration histories measured during test 9 at the ground, first, second and upper floor of the Augusta building (stations GFL-25X, 1FL-25X, 2FL-25X, 3FL-X, Fig. 3(a)). The recorded response is dominated by the isolation mode response (the isolation period can be read easily in all traces) and by higher frequency components which attenuate with distance and time. The excitation of the structural modes during the experiment is attributed to the test configuration. The response of the foundation, lying below the isolation level, as well as the transverse response, although not shown herein were insignificant. The Fourier analysis of the recorded acceleration signals shows that those are very similar in the neighborhood of the fundamental frequency (isolation frequency), which is approximately equal to f_{is} = 0.61Hz, Fig. 5(e). The following Fourier amplitude peaks are located in the higher frequency range and correspond to the higher modes of the system. Observation of Fig. 5(e) shows that the frequencies that dominate the superstructure response are mainly four and equal to f = 6.5, 13.3, 19 and 31.7Hz.

3. Signal processing

3.1 Strong motion duration

Accelerograms contain the information from the time that the induced motion exceeds the threshold trigger of the accelerometer, until the time that the recording returns to the level of the background noise. However, only some portion of the recorded vibration contributes significantly to the energy induced to the system and hence influences the system response. Duration and amplitude are the two major characteristics of any strong motion. The duration of strong motion plays a major role in the inelastic response of rigid and relatively weak structures and in the dynamic response of structures with stiffness and strength degrading characteristics. While the amplitude of the motion is a property easily quantifiable, for example the peak ground acceleration can be read immediately from the accelerogram, the duration of the motion cannot be determined straightforwardly. During the last 50 years, researchers have developed different methods for the evaluation of the strong motion classified in bracketed, uniform and significant durations, [8]. For instance, Trifunac and Brady defined the significant duration of an earthquake as the time interval during which the integral of the squared acceleration grows from 5 to 95% of its maximum value [9]. In a similar approach, herein t_d is determined as the time interval during which the cumulative squared acceleration *CSA(t)* grows rapidly, Eq. (1). For convenience, the cumulative squared acceleration *CSA(t)* is normalized to its maximum value, $CSA_n(t)$. The motion is considered to be initialized at time t_1, when the rate of change of $CSA_n(t)$ becomes factually different from zero. Fig. 6(a) shows the acceleration trace recorded during test 9 at the ground floor of the Augusta building in the time interval [1013.5, 1019]sec. The full length of the acceleration record in time is 1145sec ≈19min. Fig. 6(b) shows the corresponding normalized cumulative squared acceleration, $CSA_n(t)$, estimated according to Eq. 1. Fig.6(c) shows the rate of change of $CSA_n(t)$ in the time range [1014,1014.4]sec. The time derivative of $CSA_n(t)$ was evaluated approximately, implementing the '*diff*' function in MATLAB (sampling frequency was 1000Hz). The strong motion starts at time t_1=1014.09sec when $dCSA_n(t)/dt$ becomes greater than the selected threshold ε_1=0.01. The threshold ε_1 should chosen individually for every signal, to ensure reliable estimates of the times t_1.

$$CSA(t) = \int_0^t a(\tau)^2 d\tau, \quad CSA_n(t) = \int_0^t a(\tau)^2 d\tau \Big/ \int_0^{t_{\max}} a(\tau)^2 d\tau, \quad 0 \le CSA_n(t) \le 1 \qquad (1)$$

During motion the initial input energy transforms to kinetic energy, elastic strain energy in the superstructure and dissipated energy in the isolation system. The kinetic energy and strain energy of the vibrating system are dissipated by various damping mechanisms. The dissipation of the initial input energy marks the end of growth of the cumulative squared acceleration curve. Nevertheless, as seen in Fig. 6(b) the selection of the time when the CSA_n stops growing is very subjective. To obtain a reliable estimate of the end time of motion, the end time t_2 is estimated on the basis of the raw velocity. Fig. 7(a) shows the velocity trace derived from integration of the unprocessed ground floor acceleration, shown in Fig. 6(a), in the time interval [1014, 1030] sec. A straight line is fitted in the range [1020, 1030] sec using the '*polyfit*' function in MATLAB [10]. The fitted line is extended to the time interval [1014, 1020] sec. The linear trend observed in the velocity trace after 1020sec indicates that the motion has already ended. This is because after cessation of motion the return of the signal to the background noise level causes a shift in the acceleration baseline that translates to a linear trend in the velocity. The motion is thought to have stopped when the velocity trace $v_{raw}(t)$ distances from the linear trend $v_{linear}(t)$ by a very small quantity ε_2. The distance between the two curves is evaluated as $d_v(t) = | v_{raw}(t) - v_{linear}(t) | / v_{raw}^{\max}$, where $v_{raw}^{\max} = 0.156 m/\sec$ is the peak unprocessed velocity in the essential time frame of motion. Setting a threshold of ε_2 =0.001, the end time for the ground floor acceleration recorded during test 9 is estimated to t_2=1018sec.

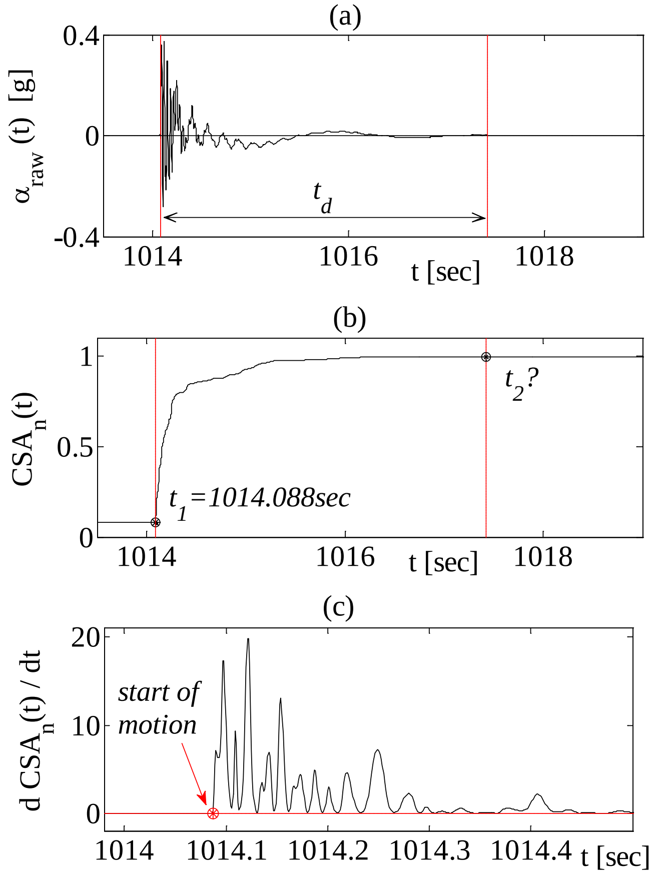

Fig. 6 – (a) Unprocessed ground floor acceleration in the time window [1013.5,1019]sec (component GFL-25X, test 9). (b) Normalized cumulative squared acceleration, $CSA_n(t)$, evaluated according to Eq. 1. (c) Rate of change of $CSA_n(t)$. The motion starts at time t_1 = 1014.088sec, when $dCSA_n(t)/dt$ becomes larger than ε_1=0.01.

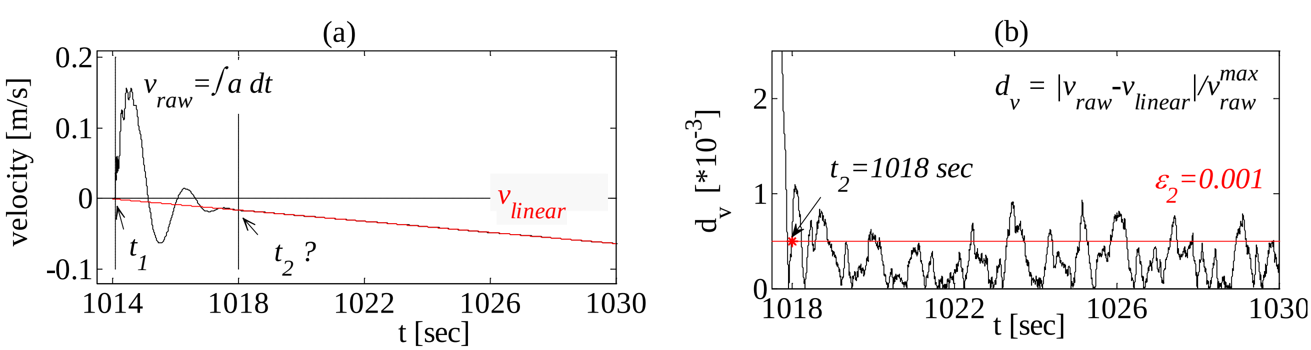

Fig. 7 - (a) Unprocessed ground floor velocity v_{raw} (t) for test 9. A straight line, v_{linear}(t), is fitted in the time interval [1020,1030]sec and extended until time t_1. (b) Distance d_v (t) between the two curves, v_{raw}(t) and v_{linear}(t), in the time interval [1017.5,1030]sec. v_{raw}^{max} is the peak value of the raw velocity. The motion ceases at time t_2=1018sec, when d_v becomes smaller than the selected threshold ε_2=0.001.

3.2 Background noise

The parts of the recorded motion preceding and following the main event are identified as pre- and post-event noise respectively. Fig. 8 shows the background noise recorded during test 9. At time t=0sec the accelerometer is enabled and starts recording the background noise (wind, traffic effects, etc.). At time t=252sec the pushing device

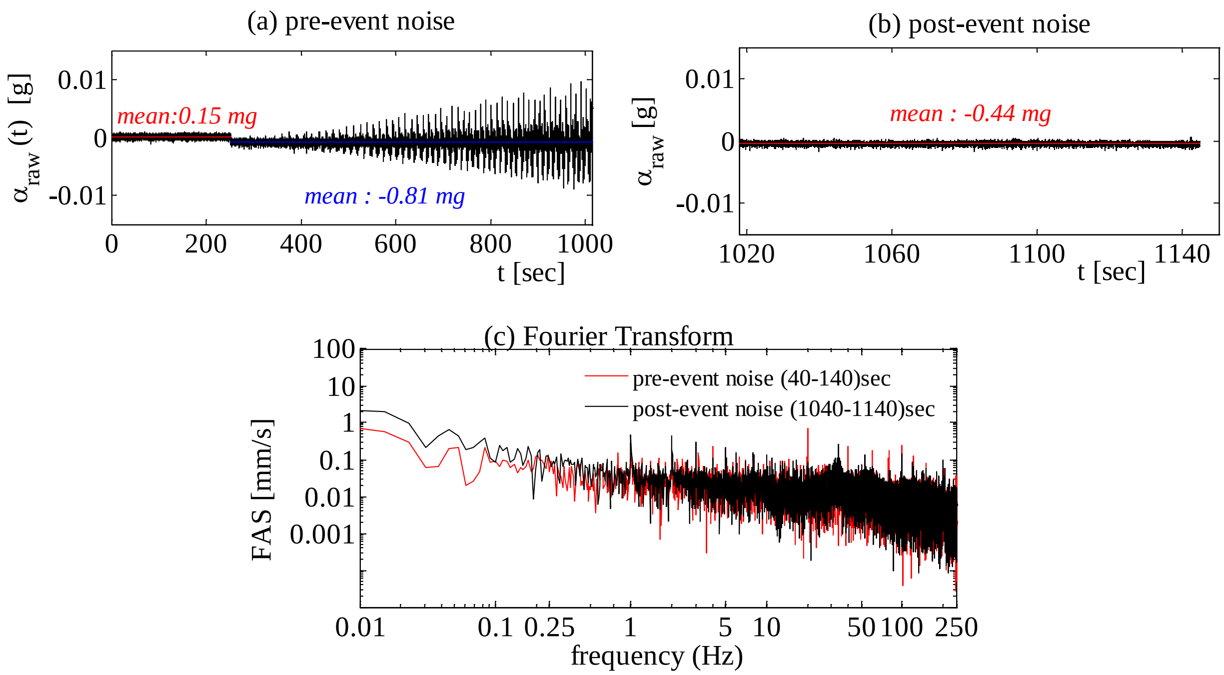

Fig. 8 – Background noise in the ground floor acceleration record obtained from test 9. (a) Pre-event noise and corresponding mean in the intervals [0,252]sec and [252,1014.09]sec. (b) Post-event noise and corresponding mean. (c) Fourier Amplitude Spectra of the background noise in the intervals [40,140]sec and [1040,1140]sec.

starts moving slowly the building. The quasi-static motion results to the slow motion noise in the interval [252,1014]sec. The slow motion noise is characterized by a very small amplitude and many acceleration spikes.

At time t=1014sec the system is released and starts vibrating. At time t=1018sec the building stops vibrating and the record returns to the level of background noise. The pre-event noise in the interval [0, 252]sec is very similar to the post-event noise, interval [1018, 1144]sec. The pre- and post-event noise is characterized by small amplitude (<10mg) and broadband frequency content. The Fourier Amplitude Spectra for the background noises are shown in Fig. 8(c). For the evaluation of the FAS of pre- and post- event noise, two samples of records are considered in the intervals [40, 140]sec and [1040, 1140]sec respectively. The two FAS are almost identical in the frequency range [0.25, 250]Hz. Some differences arise in the low frequency range (<0.25Hz), where the low frequency components of the post-event noise are more powerful than the low frequency components of the pre-event noise (the fading motion is responsible for this phenomenon). The effect of low frequency noise is more critical than the effect of the high frequency noise in the evaluation of the response quantities of interest (velocities, displacements). High frequency components attenuate with integration and therefore shall be not treated herein. It is important to note at this point that the model of the main event noise might be different than the background noise model. The need for removal of the low frequency noise becomes clear once the strong motion acceleration is integrated to provide velocities and displacements. Figs 10 and 11 show the processed absolute system response together with the corresponding raw response. The raw acceleration signal recorded at the ground floor of the Augusta building during test 9 was integrated to generate total velocities and displacements. The initial displacement, u_0=10.1cm, was added to the displacement trace obtained from integration to account for the displaced configuration of the system at t=0. The baseline shift in the raw acceleration trace is not appreciable in the scale of Fig. 10(a). However, upon integration the long period noise is amplified leading to unrealistic velocities and displacements, see Figs 10(b) and 11(a). At the end of motion the raw velocity is significantly lower than zero (-1.7cm/sec, Fig. 10(b)) and the raw residual displacement is significantly higher than the observed one (4.7cm against 1.7cm, Fig. 11(a)).

3.3 Removal of the long period noise from the main event

Once the background noise is removed from the recorded signal, the main event is adjusted. Boore in [2] suggests that the term 'signal adjustment' is more proper than the term 'correction', since the term 'correction' implies that the real signal is known and therefore can be recovered, that is seldom the case in reality. The long period noise is removed from the acceleration, velocity and displacement traces by fitting the baseline with polynomial curves of increasing order, Eqs 2.

$$\ddot{u}(t) = \ddot{u}_{raw}(t) + 2p_2 + 6p_3 t + 12p_4 t^2 + 20p_5 t^3 \tag{2a}$$

$$\dot{u}(t) = \int_0^t \ddot{u}_{raw}(\tau)d\tau + p_1 + 2p_2 t + 3p_3 t^2 + 4p_4 t^3 + 5p_5 t^4 \tag{2b}$$

$$u(t) = \int_0^t \int_0^{\tilde{\tau}} \ddot{u}_{raw}(\tau)d\tau d\tilde{\tau} + p_0 + p_1 t + p_2 t^2 + p_3 t^3 + p_4 t^4 + p_5 t^5 \tag{2c}$$

where $\ddot{u}_{raw}(t)$ is the unprocessed acceleration record and $\ddot{u}(t), \dot{u}(t), u(t)$ are the processed acceleration, velocity and displacement histories. The six coefficients p_i *(i=1,2,..6)* are evaluated explicitly from the boundary conditions, Eq. (3). Implementation of Eq.(3) into Eqs (2) leads to the system of Eq. (4), which can be easily solved for the vector of correction coefficients $\boldsymbol{p}$. t_d is the signal duration evaluated according to section 3.1.

$$\ddot{u}(0) = \ddot{u}(t_d) = 0, \quad \dot{u}(0) = \dot{u}(t_d) = 0, \quad u(0) = u_0, \; u(t_d) = u_{res} \tag{3}$$

$$\mathbf{A}\,\mathbf{p} = \mathbf{b} \tag{4}$$

$$\mathbf{A} = \begin{bmatrix} 1 & 0 & 0 & 0 & 0 & 0 \\ 0 & 1 & 0 & 0 & 0 & 0 \\ 0 & 0 & 1 & 0 & 0 & 0 \\ 1 & t_d & t_d^2 & t_d^3 & t_d^4 & t_d^5 \\ 0 & 1 & 2t_d & 3t_d^2 & 4t_d^3 & 5t_d^4 \\ 0 & 0 & 2 & 6t_d & 12t_d^2 & 20t_d^3 \end{bmatrix}, \quad \mathbf{p} = \begin{pmatrix} p_0 \\ p_1 \\ p_2 \\ p_3 \\ p_4 \\ p_5 \end{pmatrix}, \quad \mathbf{b} = \begin{pmatrix} u_0 \\ 0 \\ -\frac{1}{2}\ddot{u}_{raw}(0) \\ u_{res} - \int_0^{t_d}\int_0^{\tilde{\tau}} \ddot{u}_{raw}(\tau)\,d\tau\,d\tilde{\tau} \\ -\int_0^{t_d} \ddot{u}_{raw}(\tau)\,d\tau \\ -\ddot{u}_{raw}(t_d) \end{pmatrix} \tag{5}$$

4. Numerical applications

4.1 Baseline fitting of the absolute system response obtained from test 9

The procedure described in section 3 is implemented herein for the adjustment of the absolute accelerations recorded at the Augusta building during test 9 and the prediction of realistic floor velocities and displacements. Table 1 shows the signal durations of the test 9 records and the thresholds used in the definition of the start and end times t_1 and t_2. A delay of motion is observed as the waveform travels to the upper floors of the Augusta isolated structure. The start time t_1 of the main event is evaluated considering the time when the cumulative squared acceleration starts growing rapidly, while the end time of the main event is marked as the time when the background noise is the main constituent of the record, see Figs 9.

Table 1 - Start, end times and duration of the main free vibration signals obtained test 9 in the Augusta building. The thresholds ε_1 and ε_2 used in the determination of times t_1 and t_2 are also given.

Acceleration record	**t_1 [sec]**	**t_2 [sec]**	**t_d=t_2-t_1 [sec]**	**ε_1 [%]**	**ε_2 [%]**
Test 9 - ground floor	1014.09	1018.00	3.91	1.0	0.10
Test 9 - first floor	1014.09	1018.05	3.96	2.0	0.10
Test 9 - second floor	1014.11	1018.17	4.06	10.0	0.20
Test 9- roof	1014.12	1018.22	4.10	12.0	0.20

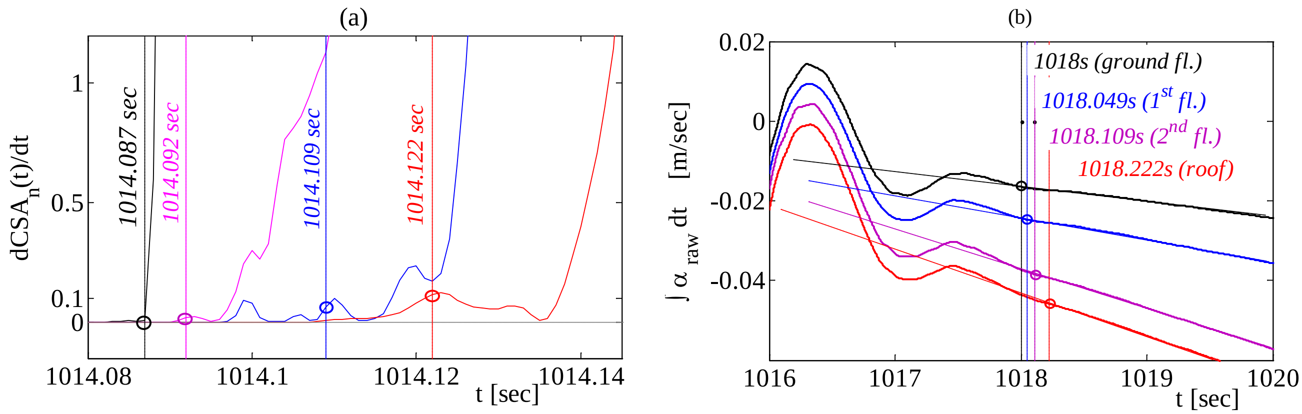

Fig. 9- (a) Rate of change of the normalized cumulative squared floor accelerations obtained from test 9 (ground floor - black line, first floor - pink line, second floor - blue line and roof - red line). The motion starts when $dCSA_n(t)/dt$ becomes greater than the corresponding threshold ε_1, see Table 1. (b) Unprocessed floor velocities. The motion stops when the raw velocity waveform starts to fit a linear trend (dashed lines).

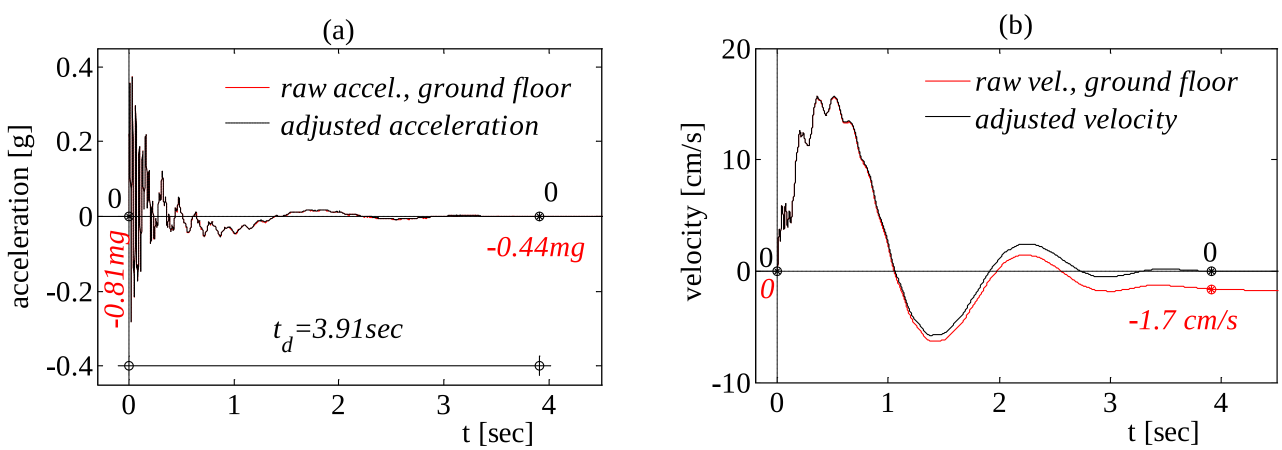

Fig. 10 - (a) Raw and adjusted ground floor acceleration for test 9. (b) Raw and adjusted ground floor velocity.

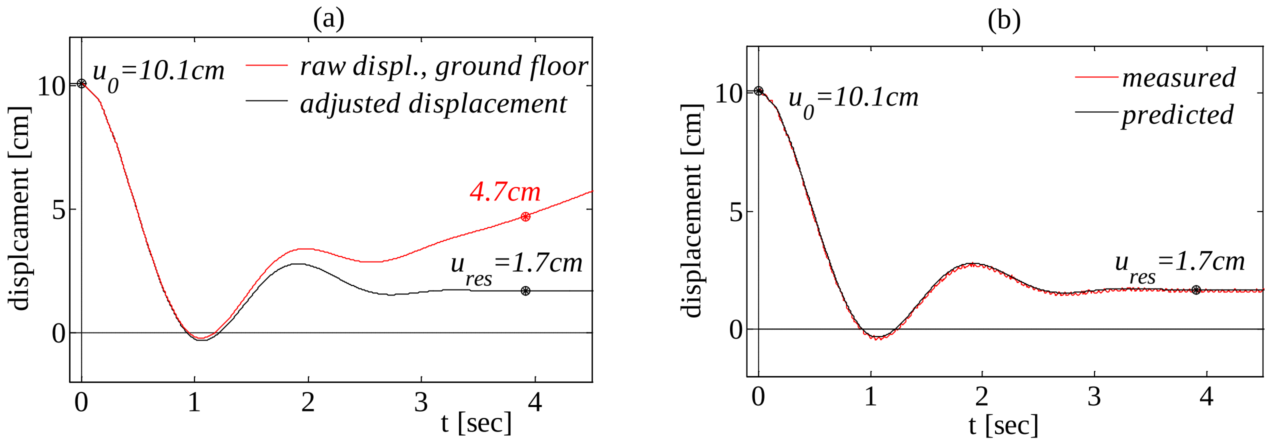

Fig. 11 - (a) Raw and adjusted ground floor displacement for test 9. (b) Comparison of the adjusted (predicted) and measured displacements.

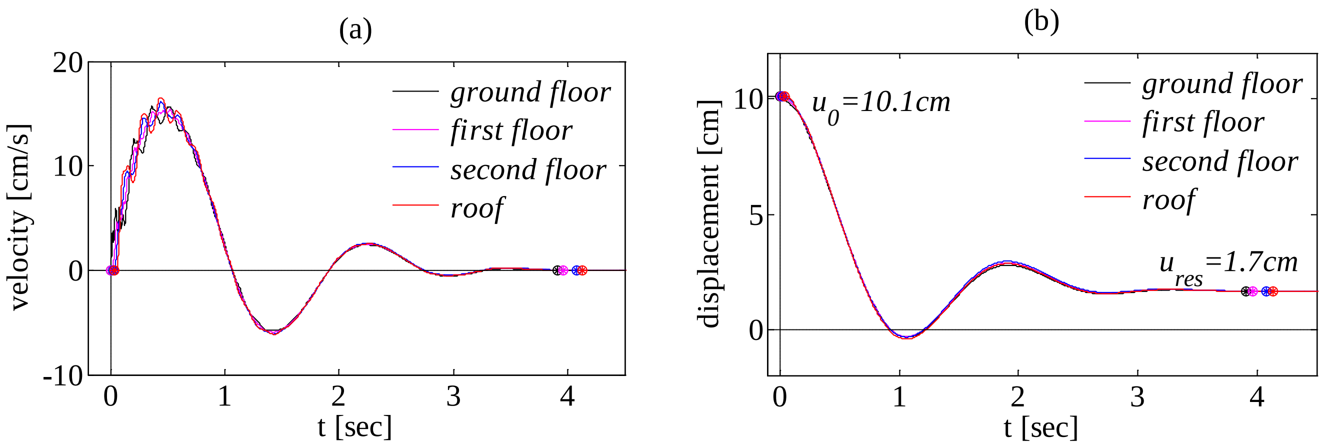

Fig. 12 - Adjusted absolute velocities and displacements at the Augusta building for test 9; sub-plots (a) and (b) respectively. The times when motion starts and ceases are indicated by markers.

Once the main event is identified, the low frequency noise is removed from the raw signals using the scheme proposed in section 3.3. The adjusted ground floor response is compared to the unprocessed signals, see Figs 10 and 11. The predicted ground floor displacement is very similar to the measured displacement, Fig. 11(b). The method is applied for the fitting of the upper floor signals, Figs 12. The obtained floor velocities and displacements are almost identical. This result demonstrates the effectiveness of base isolation to mitigate the seismic risk, protecting the superstructure.

4.2 Baseline fitting of the relative system response observed during test 9

The signal processing scheme is repeated for the processing of the relative motion observed during test 9 in the Augusta superstructure. The adjusted relative response can be evaluated in two ways:

(i) using the adjusted absolute response shown in the previous section and subtracting the ground floor response from the upper floor response, or

(ii) fitting the raw relative motion.

Table 2 provides information on the duration of the relative signal, when this is treated according to method (ii). The relative superstructure response evaluated from the adjusted absolute response (case i) is shown in Figs

13(a), 14(a), 15 (a); while the relative superstructure response evaluated from the processing of the raw relative motion response (case ii) is shown in Figs 13(b), 14(b), 15 (b). Both approaches provide similar results, enforcing the reliability of the method. Nevertheless, it should be added that the displacement traces shown in Fig. 15 were high-pass filtered at 0.3Hz, in order to provide realistic estimates of the relative displacements at the second half of motion. The need for further filtering of the displacement raises uncertainty on the reliability of the predicted relative displacements versus the end of motion. However, such uncertainty cannot be avoided since the signal-to-noise ratio tends to be significantly low for such small amplitude motions.

Table 2 - Start, end times and duration of the relative accelerations signals obtained from test 9. The thresholds ε_1 and ε_2 used in the determination of times t_1 and t_2 are also shown. The relative motion duration, when this is evaluated on the basis of the fitted absolute response, is provided within brackets.

Acceleration record	**t_1 [sec]**	**t_2 [sec]**	**t_d=t_2-t_1[sec]**	**ε_1 [%]**	**ε_2 [%]**
Test 9- first floor	1014.09	1018.15	4.06 (3.96)	2.0	0.60
Test 9- second floor	1014.09	1018.17	4.08 (4.08)	2.0	1.20
Test 9- roof	1014.09	1018.21	4.12 (4.13)	2.0	0.20

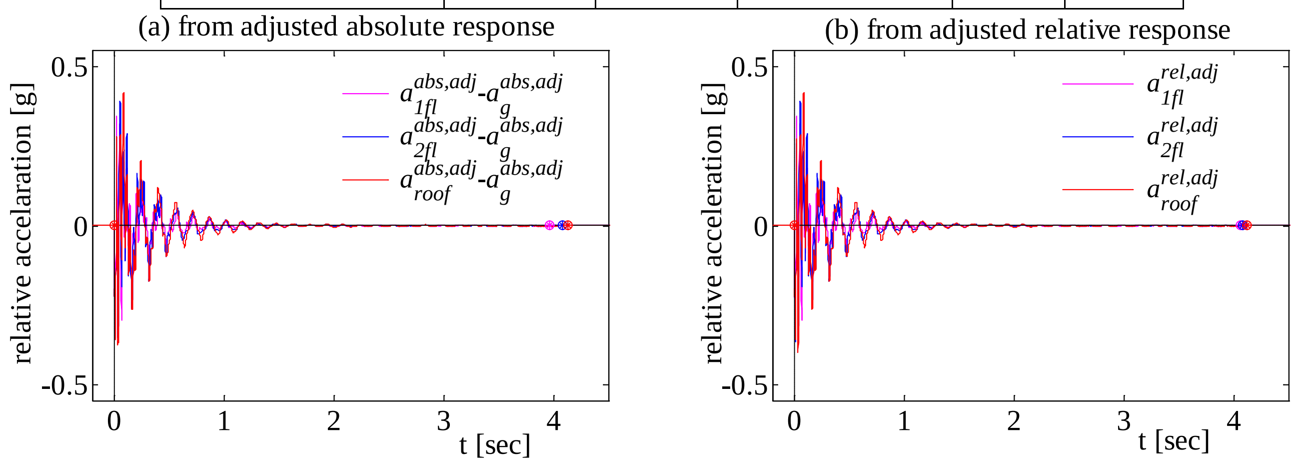

Fig. 13 - Adjusted relative floor accelerations evaluated (a) from the adjusted absolute response and (b) fitting the raw relative accelerations.

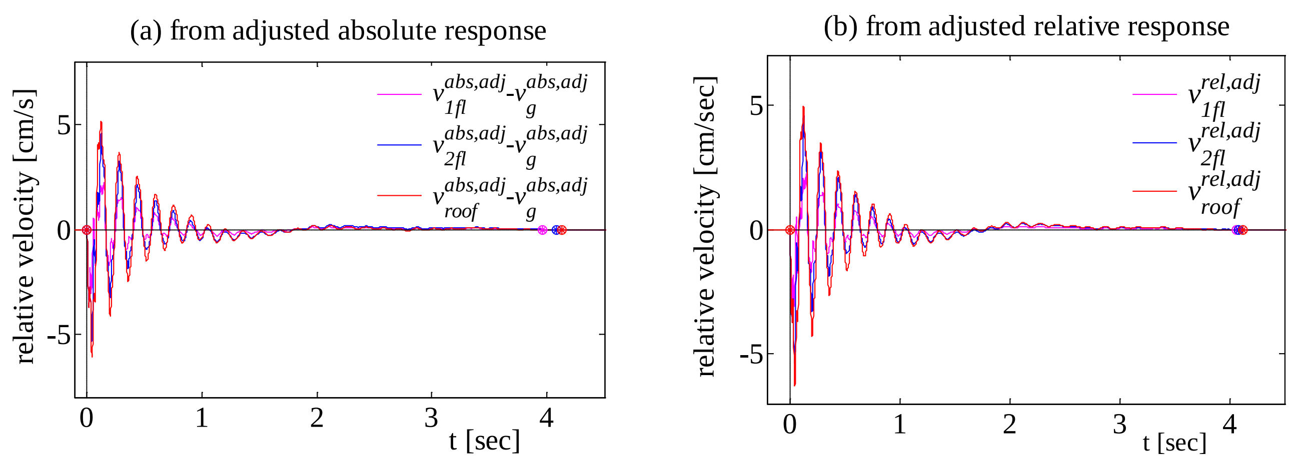

Fig. 14 - Adjusted relative floor velocities evaluated (a) from the adjusted absolute response and (b) fitting the raw relative velocities.

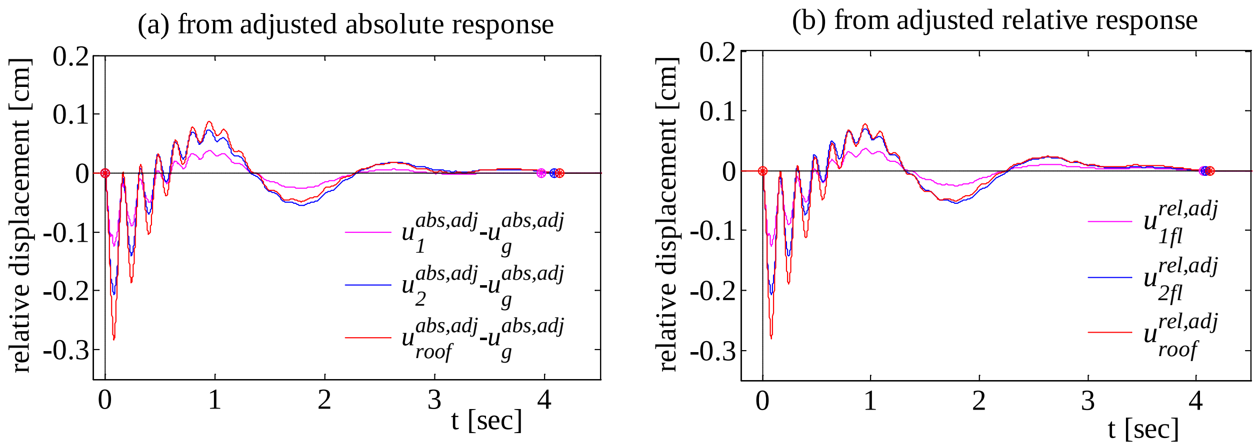

Fig. 15 - Adjusted relative floor displacement evaluated (a) from the adjusted absolute response and (b) fitting the raw relative displacements. The displacements were high pass filtered at 0.30 Hz.

4. Conclusions

A simple baseline fitting scheme is proposed herein for the adjustment of the absolute and relative acceleration signals obtained from one free vibration test performed on a base isolated building in Augusta, Sicily in 2013. The method provides reliable results, without requiring significant computational effort. One of its main advantages is the fact that it accounts for initial and end conditions. Hence, the method can recover permanent displacements, provided that these can be measured. The baseline fitting procedure proposed makes use of polynomials of increasing order for the correction of the distorted acceleration, velocity and displacement baselines. The polynomial coefficients are determined directly from the boundary conditions; namely the initial and end accelerations, velocities and displacements. The processing of the recorded data is performed in the time interval (t_1, t_2), where the motion is significant. The start time of the strong motion, t_1, is evaluated on the basis of the cumulative squared acceleration diagram CSA; t_1 is the time when CSA starts growing rapidly. The end time t_2 is selected as the time when the raw velocity trace starts to show a linear trend, which is an indication of the presence of the post-event noise. Although there is always subjectivity in the selection of the start and end times of motion, reasonable estimates of the strong motion duration lead to reasonable velocities and displacements. The adjusted response includes absolute and relative floor velocities and displacements. The generation of reasonable floor velocities and displacements is essential for the assessment of the building structural performance, since this is structural information that is not measured during the experiments. The relative displacements and drifts are evaluated in two ways: (i) subtracting the adjusted ground floor response from the adjusted upper floor response and (ii) processing the raw relative motions. The implementation of methodologies (i) and (ii) provide identical relative accelerations and velocities, enforcing this way the reliability of the method. The relative displacements are high pass filtered to remove the effects of the noise in the second half period of motion, where the signal amplitude is significantly small and the effect of the noise is predominant.

5. Acknowledgements

This work was performed with the financial support of ReLUIS (Italian National Network of University Earthquake Engineering Laboratories), ‘Project D.P.C-ReLUIS 2014–2016, WP1’.

6. References

[1] Chiu H C (1997): Stable baseline correction of digital strong-motion data. *Bulletin of the Seismological Society of America* **87**(4), 932-944.

[2] Boore D, Bommer J (2005): Processing of strong-motion accelerograms: Needs, options and consequences. *Soil Dynamics and Earthquake Engineering* 25, 93-115.

[3] Trifunac M, Lee V (1973): Routine computer processing of strong-motion accelerograms. *Tech. rep. EERL 73-03*. Earthquake Engineering Research Laboratory, Pasadena, California.

[4] EN1998 (2005): Eurocode 8. Design of Structures for Earthquake Resistance. European Committee for Standardization.

[5] Oliveto G, Athanasiou A (2014). Simulation of the response of a hybrid base-isolated building during push and quick-release tests. *2ECEES*, Istanbul, Turkey.

[6] Oliveto G, Markou A (2014): The dynamics of a pushing and quick release device for dynamic testing of seismic isolated buildings. *2ECEES*, Istanbul, Turkey.

[7] Chopra A (2012): *Dynamics of Structures. Theory and Applications to Earthquake Engineering*. 4th edition. Prentice-Hall, Inc., NJ.

[8] Boore D (2013): Fundamentals of Seismology and Seismic Hazard Assessment. Measures of strong motion and processing of data. ROSE School, Engineering Seismology Class Lecture (available online).

[9] Trifunac M, Brady A (1975): A study on the duration of strong earthquake ground motion. *Bulletin of the Seismological Society of America* **65**(3) 581-626.

[10] MATLAB, R2016a. The MathWorks Inc.